

RESEARCH LETTER

10.1002/2016GL068108

Key Points:

- Considering snow cover and sea ice together creates more skillful subseasonal forecasts
- Sea ice and snow cover influences on winter weather share a common mechanism but differ in timing
- The Arctic has a detectable influence on midlatitude weather in present and likely future climates

Supporting Information:

- Letter S1
- Figures S1 and S2 Captions and Table S1 Caption
- Figure S1
- Figure S2
- Table S1

Correspondence to:

J. C. Furtado,  
jfurtado@ou.edu

Citation:

Furtado, J. C., J. L. Cohen, and E. Tziperman (2016), The combined influences of autumnal snow and sea ice on Northern Hemisphere winters, *Geophys. Res. Lett.*, 43, doi:10.1002/2016GL068108.

Received 5 FEB 2016

Accepted 21 FEB 2016

Accepted article online 24 FEB 2016

The combined influences of autumnal snow and sea ice on Northern Hemisphere winters

J. C. Furtado<sup>1</sup>, J. L. Cohen<sup>2</sup>, and E. Tziperman<sup>3</sup>

<sup>1</sup>School of Meteorology, University of Oklahoma, Norman, Oklahoma, USA, <sup>2</sup>Atmospheric and Environmental Research, Lexington, Massachusetts, USA, <sup>3</sup>Department of Earth and Planetary Sciences and School of Engineering and Applied Sciences, Harvard University, Cambridge, Massachusetts, USA

**Abstract** Past studies have demonstrated a significant relationship between the phase and amplitude of the Northern Annular Mode (NAM) and both Arctic sea ice and high-latitude snow cover during boreal autumn. However, those studies have considered these forcings separately. Here we consider the collective effect of Arctic sea ice and snow cover variability for producing skillful subseasonal forecasts for Northern Hemisphere (NH) winter conditions. We find that these two cryospheric elements interact with the extratropical atmosphere differently through the cold season. Sea ice extent minima during November play a role in stratospheric and tropospheric circulation anomalies during November/December with a secondary maximum in late January/February. October snow cover anomalies, however, have impacts on the NAM primarily during middle to late winter. These timing differences are likely tied to differences in anomalous wave driving between the two cases, though other processes may be in play. We exploit these different influences to produce a skillful forecast model of subseasonal NH surface temperatures using both sea ice and snow cover as predictors, with large gains in skills in January. Overall, our study suggests that the Arctic has a demonstrable and detectable influence on midlatitude winter weather in the present and likely future climate.

1. Introduction

Attention on the role of the Arctic in influencing Northern Hemisphere (NH) midlatitude weather regimes has increased with the emergence of Arctic Amplification—i.e., the rapid warming of the high latitudes and diminution of the Arctic cryosphere [Screen and Simmonds, 2010; Francis and Vavrus, 2012; Stroeve et al., 2012; Cohen et al., 2014a]. Several studies have specifically highlighted the roles of the melting of Arctic sea ice and extent of open waters in the Arctic Ocean [e.g., Honda et al., 2009; Liu et al., 2012; Tang et al., 2013; Kim et al., 2014; Mori et al., 2014; García-Serrano et al., 2015; King et al., 2015] and continental snow cover event (SCE), especially across Eurasia [e.g., Cohen and Entekhabi, 1999; Allen and Zender, 2010], on influencing NH extratropical atmospheric climate variability. Until recently, these two boundary forcings have been considered separately. However, observational and modeling studies suggest a similar chain of events from the fall into the winter for both snow cover and sea ice [Cohen et al., 2007; Kim et al., 2014]. Given anomalously high autumn Eurasian snow cover extent (SCE) or low Arctic sea ice extent (SIE), the chain of events is as follows: (1) amplification of the standing wave pattern over and off of Asia, (2) enhanced vertical wave propagation into the polar stratosphere, (3) weakening of the stratospheric polar vortex, and (4) subsequent equatorward displacement of the tropospheric polar jet stream, or the negative phase of the Northern Annular Mode (NAM) [e.g., Thompson and Wallace, 2000, 2001], via downward propagation [e.g., Baldwin and Dunkerton, 1999]. The similarity of the influences of snow cover and sea ice anomalies prompted a proposal of their potential collective influence on the wintertime NH extratropical circulation [Cohen et al., 2014a], which remains untested up until now.

In this study, we offer the first quantification of the combined influence of Arctic snow and sea ice covers as predictors for subseasonal (20–30 day) NH wintertime climate variability. The analysis is statistical and therefore presents suggested relationships between Arctic cryospheric anomalies and the NH wintertime circulation pattern. Nevertheless, we demonstrate improved skill in subseasonal winter forecasting, a timescale with little demonstrable forecast skill currently [Hoskins, 2013], using the Arctic cryosphere.

## 2. Data and Methods

Observations are taken from several sources. For the atmospheric fields, we use daily mean and monthly mean fields from the European Centre for Medium-Range Weather Forecasts global atmospheric reanalysis product (ERA-Interim) [Dee *et al.*, 2011]. The data are on a  $1.5^\circ$  by  $1.5^\circ$  latitude/longitude grid globally and span 23 vertical pressure levels. For our analysis, we restrict the analysis between 10 and 1000 hPa. Primary fields analyzed include sea level pressure (SLP), geopotential height, and air temperature. For the Arctic cryosphere, we use data from the Rutgers Global Snow Laboratory for SCE [Robinson *et al.*, 1993] and the National Snow and Ice Data Center [Cavalieri *et al.*, 1996] for SIE. SCE data are on an irregular  $89 \times 89$  grid, which are interpolated onto a regular  $1^\circ \times 1^\circ$  grid using bilinear interpolation. SIE data have a resolution of 25 km across the Arctic. Anomalies of all fields are computed by removing the daily and monthly mean values computed over the base period 1981–2010.

The NAM index for a given pressure level is calculated as the expansion coefficient (EC) time series computed by projecting daily mean geopotential height anomalies onto the spatial pattern of the leading empirical orthogonal function (EOF) of November–March (NDJFM) monthly mean geopotential height anomalies at that pressure level. The NAM index is subsequently standardized by removing the daily mean (1981–2010) from the index and dividing by its standard deviation.

Multivariate EOF analysis is used for assessing the covariability of the Arctic cryosphere variables and the NH wintertime circulation [e.g., Wilks, 2006]. Prior to eigenanalysis, all fields are linearly detrended and standardized. The leading mode of the multivariate EOF analysis is retained as it is significantly different from the remaining modes. Statistical significance for the multivariate EOF analysis is done through Monte Carlo simulations with randomly shuffled SLP fields in space, similar to Garcíá-Serrano *et al.* [2015]. The EC time series of October NH SCE and November Arctic SIE are derived by projecting the raw monthly anomaly fields onto the leading spatial patterns of SCE and SIE from the leading multivariate EOF analysis, respectively.

Finally, the surface temperature forecast model used in this study is a simple linear regression model that considers only the October SCE EC time series (SNOW), only the November Arctic SIE EC time series (SEAICE), or both, as predictors of the monthly mean near-surface temperature anomaly ( $T_{sfc}$ ); i.e.,  $T_{sfc} = a \times \text{SNOW} + b \times \text{SEAICE} + c$ , where  $a$ ,  $b$ , and  $c$  are coefficients determined through least squares fitting. Both SNOW and SEAICE are linearly detrended prior to least squares fitting to remove the potential impacts of trends on the joint statistics. Model skill of the hindcasts is assessed using the anomaly correlation coefficient (ACC) [Miyakoda *et al.*, 1972]:

$$\text{ACC} = \frac{\sum_{m=1}^M f'_m v'_m}{\sqrt{\sum_{m=1}^M (f'_m)^2} \sqrt{\sum_{m=1}^M (v'_m)^2}} \quad (1)$$

$$f'_m = f_m - c_m \quad v'_m = v_m - c_m$$

where  $f_m$  is the forecast value of the variable for time  $m$ ,  $v_m$  is the observed (or verified) value, and  $c_m$  is the climatological average. For model skill assessment, we employ the leave-one-out cross-validation method [e.g., Elsner and Schmertmann, 1994] for each of the forecast models (i.e., snow only, sea ice only, and both). For the leave-one-out method, we recompute the multivariate EOFs but leave out the snow, ice, and SLP anomalies associated with year  $X$  in the calculation. Then, the EC time series of October NH SCE and November Arctic SIE are computed from these new maps and are used to compute regression coefficients for the linear model. These derived regression coefficients are then used to hindcast the wintertime monthly temperature anomalies for year  $X$ . This process is repeated for every year (1979–2014) in the record. Significance values for the ACC from the model are tested using a bootstrap approach with 5000 random samples of the record with replacement.

## 3. Results

### 3.1. Multivariate EOF and Composite Analyses

Figure 1 shows the leading mode of the multivariate EOF analysis of October NH SCE (poleward of  $30^\circ\text{N}$ ), November Arctic SIE (poleward of  $60^\circ\text{N}$ ), and December–February (DJF) NH SLP (poleward of  $20^\circ\text{N}$ ) from 1979/1980 to 2014/2015. The months for SCE and SIE anomalies are chosen based on previous works on

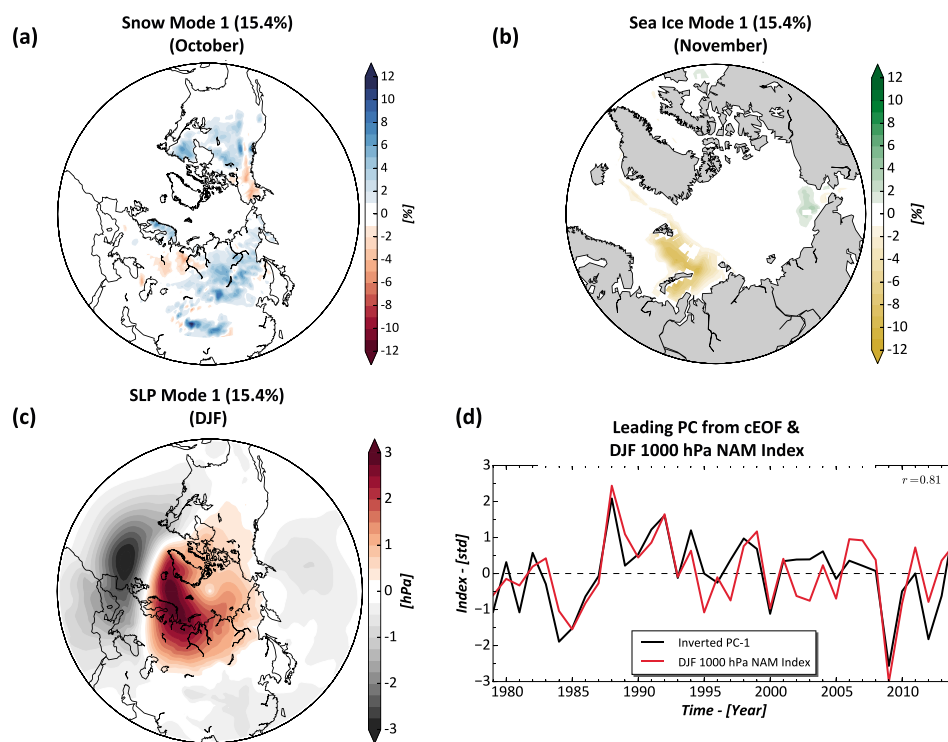


**Figure 1.** (a) Regression of October SCE anomalies (%) onto the leading principal component (PC) times series from the multivariate EOF analysis of October SCE, November Arctic SIE, and December–February (DJF) SLP. (b) As in Figure 1a but for November SIE anomalies (%). (c) As in Figure 1a but for DJF SLP anomalies (hPa). Percent variance in the three fields explained by the leading mode included in the titles of Figures 1a–1c. (d) (black) The leading PC time series (standardized and inverted) from the multivariate EOF analysis from 1979/1980 to 2014/2015. (red) The observed DJF NAM 1000 hPa index from 1979/1980 to 2014/2015. Correlation between the two plotted indices is  $r = 0.81$  ( $p < 0.01$ ).

Arctic-NH middle-latitude teleconnections [e.g., Cohen and Entekhabi, 1999; Mori et al., 2014; García-Serrano et al., 2015]. The leading mode explains 15.4% of the variance in the three fields, which is modest, but the EOF analysis includes a highly spatially variable field (i.e., snow cover). Covariability exists between anomalously high October SCE over Eurasia and North Central North America and anomalously low November Arctic SIE, particularly in the Barents-Kara (BK) Seas region (Figures 1a and 1b). These two features covary with anomalously high (low) SLP in the Arctic (middle latitudes) (Figure 1c), a pattern resembling the negative phase of the near-surface NAM. Indeed, the spatial correlation between Figure 1c and the characteristic negative NAM SLP pattern [e.g., Thompson and Wallace, 2000] is  $r = 0.90$  ( $p < 0.01$ ). Positive SLP anomalies extend into northern Eurasia more than observed with the canonical NAM signature, indicating that this leading SLP pattern likely captures variability in the Siberian High. The leading principal component (PC) time series of the multivariate EOF analysis is also strongly correlated with the observed DJF 1000 hPa NAM index ( $r = 0.81$ ;  $p < 0.01$ ) (Figure 1d). Similar conclusions arise if we restrict SCE to only Eurasia (Figure S1 in the supporting information).

Hypotheses concerning the lagged influence of autumnal SCE and SIE on the wintertime NAM suggest a subseasonal stratospheric pathway for extended predictability of NH wintertime weather [Cohen et al., 2007; Kim et al., 2014]. To evaluate the influence of October NH SCE and November Arctic SIE on subseasonal NH winter variability, we construct composites of the daily mean NAM index and vertical component of the wave activity flux (i.e., WAFz, proportional to meridional heat flux) [Plumb, 1985], area averaged from 40 to 80°N (Figure 2). High and low SCE/SIE years are chosen from the 10 highest and lowest values of the October SCE and November SIE EC time series separately (Table S1). These two indexes are virtually uncorrelated ( $r = 0.06$ ), making them independent for compositing and regression (section 3.2). Composite differences are computed as high – low for SCE and low – high for SIE to facilitate easier comparison between the two (i.e., high SCE and low SIE have a similar chain of events—see section 1). Starting with the SCE composites, significant negative NAM anomalies in the troposphere and middle stratosphere are prevalent from the end of

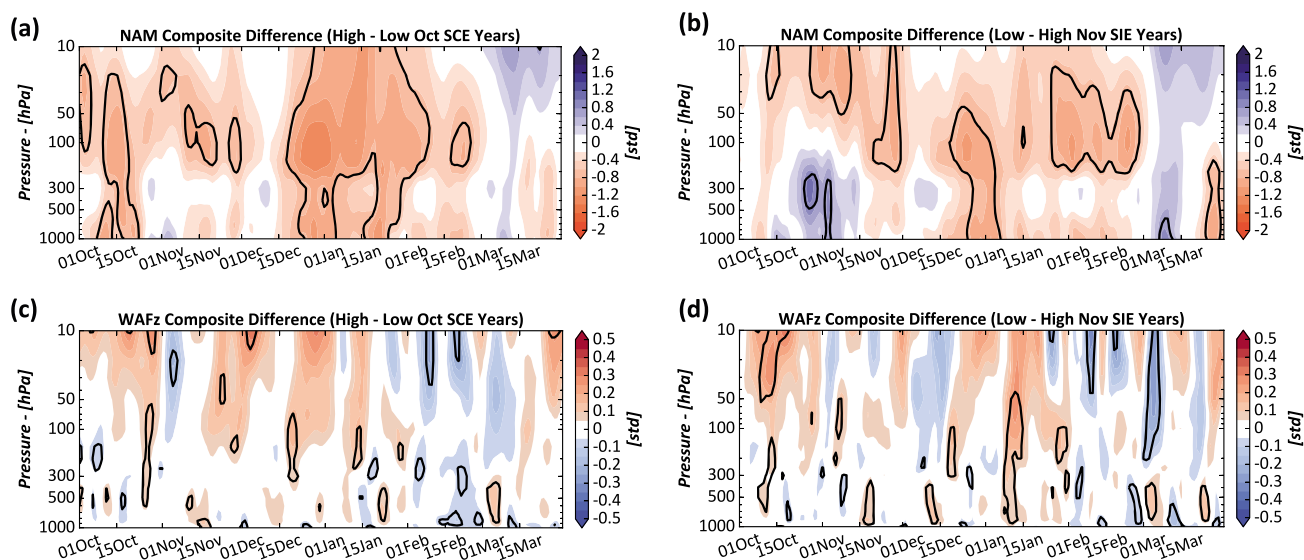


**Figure 2.** (a) Composite difference (i.e., high – low) of the standardized NAM index at each pressure level for the top 10 high and top 10 low October SCE years. (b) As in Figure 2a but composite for the top 10 low and top 10 high November SIE years (i.e., low – high). (c) As in Figure 2a but for vertical wave flux (WAFz), standardized and area-averaged 40–80°N at each pressure level. (d) As in Figure 2b but for WAFz, standardized and area-averaged 40–80°N at each pressure level. A 7 day smoother is applied to all fields prior to compositing. Black contour in all panels denotes composite differences significant at the  $p < 0.1$  level per a two-sample t test. Years used for the composites shown in Table S1.

December until early February (Figure 2a), suggesting a higher propensity for cold air outbreaks in the NH middle latitudes during years with extensive October NH SCE. A significant NAM signal is absent from November into early December in the troposphere, supporting the delayed influence of anomalous October SCE on the midwinter surface climate [e.g., Cohen *et al.*, 2014b]. The associated WAFz composite difference (Figure 2c) indicates anomalously positive meridional heat flux in the lower stratosphere in November–December. However, statistical significance is marginal, suggesting high variance in the timing and magnitude of these WAFz anomalies.

A different subseasonal evolution of the NAM and WAFz occurs when considering years of high and low Arctic SIE anomalies (Figures 2b and 2d). During Novembers with low Arctic SIE, the tropospheric and stratospheric NAMs are anticorrelated, with significant positive (negative) NAM anomalies in the troposphere (stratosphere). The negative stratospheric NAM anomalies linger and appear to descend with time during December, reaching the surface at the end of December and replacing the previous positive tropospheric NAM anomalies (Figure 2b). Negative NAM anomalies then dominate the composite difference into February, especially in the stratosphere. Stratosphere-troposphere connections related to November Arctic SIE anomalies are most robust during January, when significant and strong positive WAFz anomalies are present (Figure 2d) and precede the weakened stratospheric circulation in February (Figure 2b). Signals of wave driving during November and December are less coherent, although there is an indication for enhanced positive WAFz during low sea ice years in early December (Figure 2d).

The similarities and the differences in timing of influence between the SCE and SIE anomalies motivate an examination of how the two collectively influence the NH wintertime atmosphere. As such, we create composites using years with both anomalously high (low) October NH SCE and low (high) November Arctic SIE (see Table S1 for a list of years). The October SCE EC time series and November EC time series are virtually uncorrelated ( $r = 0.06$ ), making these two indices independent enough for the purposes of compositing and statistical modeling (see section 3.2). Figure 3 illustrates significant NAM and WAFz anomalies present when considering the collective influence of SCE and SIE. A coherent negative NAM signal during high October SCE, low November SIE years emerges in the polar stratosphere in early November and joins with same-signed tropospheric anomalies in late December (Figure 3a). Significant positive WAFz anomalies during November (Figure 3b) are also observed and further support the importance of the stratosphere-troposphere dynamical coupling mechanism [e.g., García-Serrano *et al.*, 2015]. When comparing and contrasting Figures 2 and 3, the two cryospheric components work in concert to enhance the NAM signal from December through January, suggesting the potential for improved NH weather forecast skill during early and middle winter.

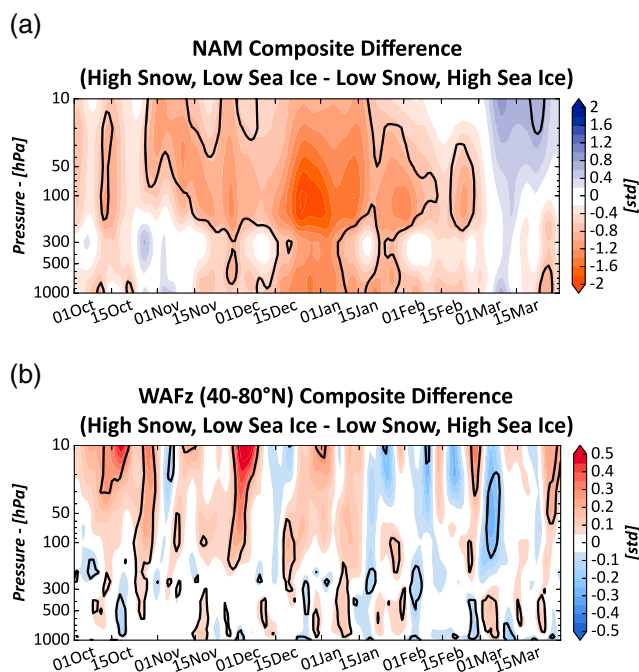


**Figure 3.** (a) Composite difference (i.e., high snow/low sea ice years – low snow/high sea ice years) of the standardized NAM index at each pressure level. (b) As in Figure 3a but for vertical wave flux (WAFz), standardized and area-averaged 40–80°N at each pressure level. A 7 day smoother is applied to all fields prior to compositing. Black contour in all panels denotes composite differences significant at the  $p < 0.1$  level per a two-sample  $t$  test. Years used for the composites shown in Table S1.

One caveat of the analysis is the relatively small sample size—only 7 years exist in each of the high October SCE, low November SIE and low October SCE, high red November SIE bins ( $N = 12$  for statistical testing of composite differences). Thus, our results are strongly suggestive but not wholly conclusive and will benefit from more samples in the future.

### 3.2. Use of Snow Cover and Sea Ice in a Simple Forecast Model

Our analysis thus far indicates the potential for enhanced subseasonal forecast skill for NH wintertime climate via coherent signals in the tropospheric and stratospheric NAM when considering both autumnal SCE and SIE. To relate our results to sensible weather, Figure 4 presents the leading patterns of the multivariate EOF of October NH SCE, November Arctic SIE, and wintertime  $T_{\text{sfc}}$  anomalies. The multivariate EOF analysis using DJF  $T_{\text{sfc}}$  anomalies (Figure 4c) indicates that October NH SCE and November Arctic SIE covary strongly with a hemispheric-wide temperature anomaly pattern like that associated with the negative phase of the NAM [e.g., Thompson and Wallace, 2000, 2001]. Analyzing each winter month separately, however, shows interesting spatial differences (Figures 4d–4f). Large negative  $T_{\text{sfc}}$  anomalies are focused in the center of the NH continents, with a westward (eastward) spread of the cold anomalies across Eurasia (North America) as the winter progresses. For example, early season cold air outbreaks in North America during high October SCE/low November SIE years are more likely in Central Canada and the U.S., whereas late-season cold outbreaks encompass the eastern U.S. (Figures 4d–4f). Indeed, when examining specific winters that featured both anomalously high October NH SCE and anomalously low November Arctic SIE (i.e., those years composited in Figure 3), the composite  $T_{\text{sfc}}$  anomalies for each month and the season resemble closely the patterns obtained from the multivariate EOF analysis (Figure S2).

Finally, we evaluate the predictive skill of SCE and SIE for NH monthly mean  $T_{\text{sfc}}$  anomalies using the detrended October SCE EC time series and November SIE EC time series separately and together as predictors (Figure 5) in a simple linear regression model (see section 2). Our intent is not to argue that variations in the Arctic cryosphere are the *only* controls on NH winter climate. Instead, we wish to demonstrate that the autumn Arctic cryosphere contains significant predictive information for the large-scale NH circulation pattern that can impact wintertime temperature (and precipitation) patterns. The highest (lowest) hemispheric-scale model skill occurs in January (December) (Figures 5a, 5d, and 5g and Figures 5b, 5e, and 5h), in agreement with the

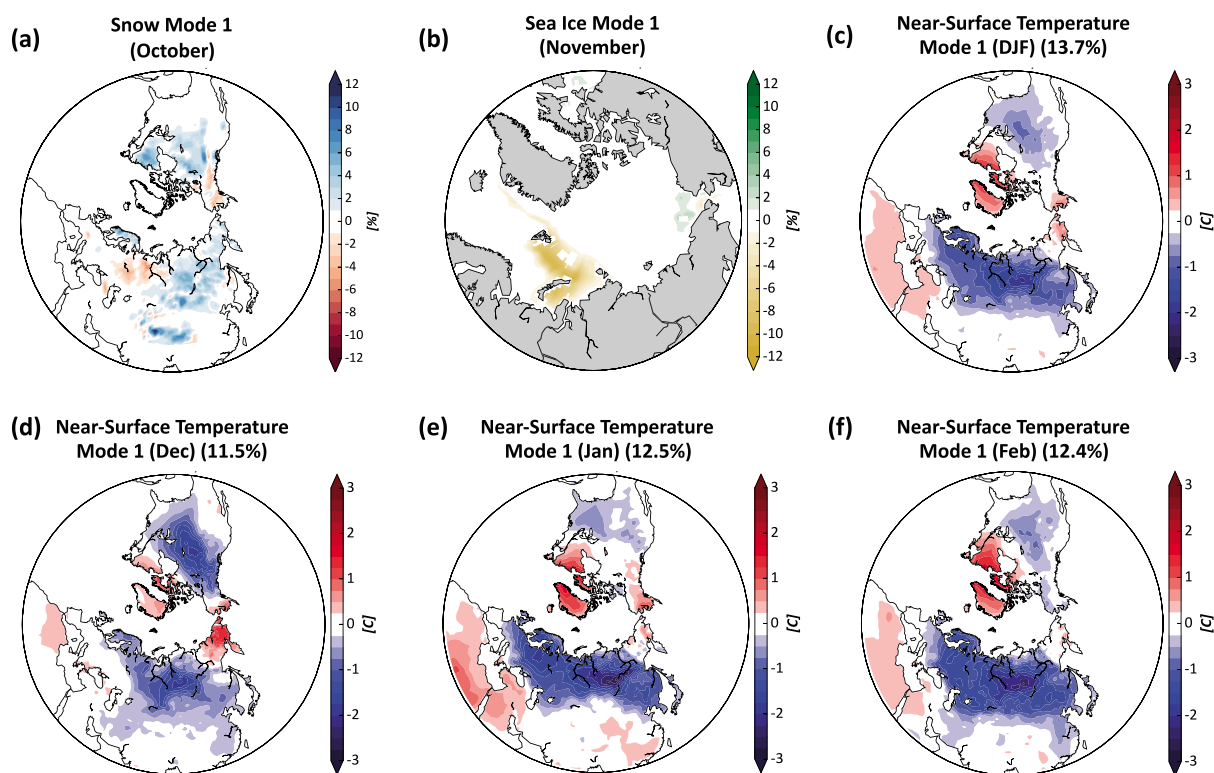


**Figure 4.** Regression of (a) October NH SCE anomalies (%), (b) November Arctic SIE anomalies (%), and (c) DJF near-surface temperature ( $T_{\text{sfc}}$ ) anomalies ( $^{\circ}\text{C}$ ) onto the leading principal component (PC) time series of the multivariate EOF of those three fields. (d) As in Figure 4c but for the PC time series from the multivariate EOF analysis using December  $T_{\text{sfc}}$  anomalies. (e) As in Figure 4d but for the PC time series from the multivariate EOF analysis using January  $T_{\text{sfc}}$  anomalies. (f) As in Figure 4d but for the PC time series from the multivariate EOF analysis using February  $T_{\text{sfc}}$  anomalies. Percent variance explained by the leading mode shown in Figures 4c–4f.

NAM and WAFz composite differences (Figures 2 and 3). Moreover, the hemispherically averaged skill is generally higher when both October SCE and November SIE are used as predictors than each individually (Figures 5c, 5f, and 5i). This fact reaffirms our initial hypothesis that the collective influences of snow cover and sea ice have an impact on subseasonal NH wintertime circulation variability but contribute differently through the season. Regionally, four areas stand out with enhanced and significant ( $p < 0.1$ ) subseasonal  $T_{\text{sfc}}$  forecast skill when considering both cryosphere predictors: (1) the central and eastern United States, (2) the Middle East and North Africa (especially in January), (3) East Asia, and (4) Scandinavia and parts of Northeastern Europe. These regions are traditionally difficult to forecast during the winter [e.g., Hoskins, 2013; Scaife et al., 2014]. Thus, using the skillful Arctic cryosphere predictors discussed here and their influence on subseasonal variability in the NAM may offer improvement for forecast skill in those regions.

#### 4. Summary and Conclusions

Taken together, our results offer a step forward in understanding the combined effect of two cryospheric elements (October NH snow cover extent (SCE) and November Arctic sea ice extent (SIE)) on NH wintertime climate variability. Previous works have considered these forcings individually, typically on the seasonal scale. The gain in model skill (Figure 5) arises from extended subseasonal skill in NAM predictability in the stratosphere and the troposphere when considering both October SCE and November SIE anomalies (Figure 3). The mechanism for the combined influence requires further analysis given the weak WAFz composites (Figures 2c and 2d). While our results support prior studies suggesting downward propagation of stratospheric anomalies influencing the tropospheric circulation as the key mechanism, there may be important tropospheric-centric processes also at work, possibly linked to indirect changes in the tropospheric waveguide by the stratospheric circulation [e.g., Song and Robinson, 2004; Simpson et al., 2009; Garfinkel et al., 2013]. Furthermore, atmospheric and coupled general circulation models have difficulty reproducing observed cryospheric influences on the

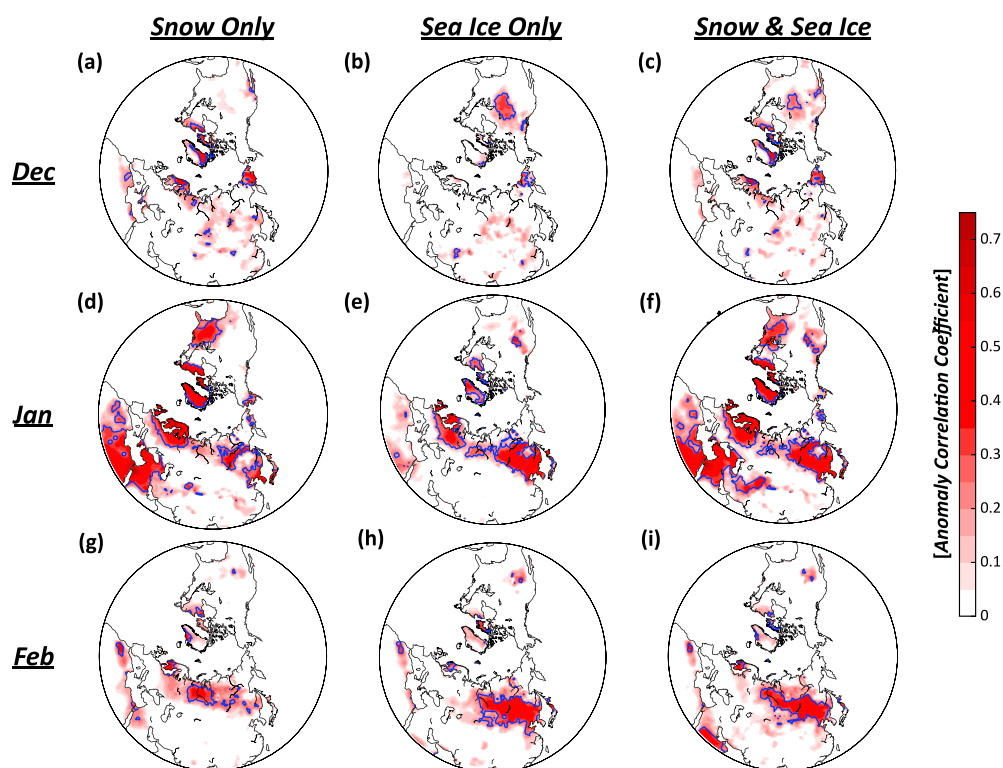


**Figure 5.** The anomaly correlation coefficient (ACC) for hindcasts of monthly mean land near-surface temperature anomalies using a linear regression model (see text) for each month. Results shown for (a–c) December, (d–f) January, and (g–i) February using hindcasts for the winters of 1979/1980–2014/2015. Three sets of predictors are used: the October NH SCE EC time series only (Figures 5a, 5d, and 5g), the November Arctic SIE EC time series (Figures 5b, 5e, and 5h), and both the October NH SCE and November Arctic SIE EC time series (Figures 5c, 5f, and 5i). Blue contour outlines where ACC values are significant at the  $p < 0.1$  level.

midlatitude atmosphere [e.g., Furtado et al., 2015; Li et al., 2015]. As such, we are unable to discount completely the role of internal atmospheric variability in driving these observed relationships.

The constructive and destructive influences of snow cover and sea ice anomalies on the phase of the wintertime NAM need to be explored dynamically to understand why the timing of the tropospheric response varies as it does. Combining our statistical results, which are limited by the relatively short length of the satellite era observational record, with such a new understanding of the interactions should improve dynamical model performance and hence confidence in their winter forecasts. Using long simulations or hindcasts from dynamical models (e.g., the North American Multi-Model Ensemble) [Kirtman et al., 2014] may also increase confidence in the relationships documented here, with the caveat that coupled climate models often poorly simulate Arctic sea ice and snow variability [Cohen et al., 2014a; Furtado et al., 2015]. Additionally, targeted modeling experiments with simultaneous changes in snow cover and sea ice are desirable to test the signals shown in this study. However, the interdependence between Arctic sea ice and continental snow cover and their connections with other large-scale climate variables (e.g., El Niño) need to be considered for operational use and general climate dynamics studies. Understanding the interplay of these multiple climate features may lead to a better dynamical interpretation of the forecast skill obtained when using the two Arctic cryosphere predictors. This type of quantification will also improve our assessment of future climate under greenhouse warming, especially as competing climatic influences may become more amplified in the future.

### References

Allen, R. J., and C. S. Zender (2010), Effects of continental-scale snow albedo anomalies on the wintertime Arctic Oscillation, *J. Geophys. Res.*, *115*, D23105, doi:10.1029/2010JD014490.  
 Baldwin, M. P., and T. J. Dunkerton (1999), Propagation of the Arctic Oscillation from the stratosphere to the troposphere, *J. Geophys. Res.*, *104*, 30,937–30,946.

### Acknowledgments

This work was supported by the National Science Foundation Large-Scale and Climate Dynamics Program (grants AGS-1303647 and AGS-1303604) and the National Science Foundation Division of Polar Programs (grant PLR-1504361). The authors also thank the Weizmann Institute for its hospitality in hosting E. Tziperman during parts of this work. All data for this paper are properly cited and referred to in the reference list. The authors would also like to thank two anonymous reviewers who provided insightful comments and constructive feedback that ultimately improved the manuscript.

- Cavalieri, D. J., C. L. Parkinson, P. Gloersen, and H. Zwally (1996), Sea ice concentrations from Nimbus-7 SMMR and DMSP SSM/I-SSMIS passive microwave data, version 1. November 1979–2014, *Tech. Rep.*, NASA Natl. Snow and Ice Data Cent. Distrib. Active Archive Cent., Boulder, Colo.
- Cohen, J., and D. Entekhabi (1999), Eurasian snow cover variability and Northern Hemisphere climate predictability, *Geophys. Res. Lett.*, *26*, 345–348.
- Cohen, J., M. Barlow, P. J. Kushner, and K. Saito (2007), Stratosphere-troposphere coupling and links with Eurasian land surface variability, *J. Clim.*, *20*, 5335–5343.
- Cohen, J., et al. (2014a), Recent Arctic Amplification and extreme mid-latitude weather, *Nat. Geosci.*, *7*, 627–637.
- Cohen, J., J. C. Furtado, J. Jones, M. Barlow, D. Whittleston, and D. Entekhabi (2014b), Linking Siberian snow cover to precursors of stratospheric variability, *J. Clim.*, *27*, 5422–5432.
- Dee, D. P., et al. (2011), The ERA-Interim reanalysis: Configuration and performance of the data assimilation system, *Q. J. R. Meteorol. Soc.*, *137*, 553–597.
- Elsner, J. B., and C. P. Schmertmann (1994), Assessing forecast skill through cross validation, *Weather Forecasting*, *9*, 619–624.
- Francis, J. A., and S. J. Vavrus (2012), Evidence linking Arctic amplification to extreme weather in mid-latitudes, *Geophys. Res. Lett.*, *39*, L06801, doi:10.1029/2012GL051000.
- Furtado, J. C., J. L. Cohen, A. H. Butler, E. E. Riddle, and A. Kumar (2015), Eurasian snow cover variability and Northern Hemisphere climate predictability, *Clim. Dyn.*, *45*, 2591–2605.
- García-Serrano, J., C. Frankignoul, G. Gastineau, and A. de la Cámara (2015), On the predictability of the winter Euro-Atlantic climate: Lagged influence of autumn Arctic sea ice, *J. Clim.*, *28*, 5195–5216.
- Garfinkel, C. I., D. W. Waugh, and E. P. Gerber (2013), The effect of tropospheric jet latitude on coupling between the stratospheric polar vortex and the troposphere, *J. Clim.*, *26*, 2077–2095.
- Honda, M., J. Inoue, and S. Yamane (2009), Influence of low Arctic sea-ice minima on anomalously cold Eurasian winters, *Geophys. Res. Lett.*, *36*, L08707, doi:10.1029/2008GL037079.
- Hoskins, B. (2013), The potential for skill across the range of the seamless weather–climate prediction problem: A stimulus for our science, *Q. J. R. Meteorol. Soc.*, *139*, 573–584.
- Kim, B.-M., S.-W. Son, S.-K. Min, J.-H. Jeong, S.-J. Kim, X. Zhang, T. Shim, and J.-H. Yoon (2014), Weakening of the stratospheric polar vortex by Arctic sea-ice loss, *Nat. Commun.*, *5*, 4646.
- King, M. P., M. Hell, and N. Keenlyside (2015), Investigation of the atmospheric mechanisms related to the autumn sea ice and winter circulation link in the Northern Hemisphere, *Clim. Dyn.*, *46*, 1185–1195, doi:10.1007/s00382-015-2639-5.
- Kirtman, B. P., et al. (2014), The North American multimodel ensemble: Phase-1 seasonal-to-interannual prediction; Phase-2 toward developing intraseasonal prediction, *Bull. Am. Meteorol. Soc.*, *95*, 585–601.
- Li, C., B. Stevens, and J. Marotzke (2015), Eurasian winter cooling in the warming hiatus of 1998–2012, *Geophys. Res. Lett.*, *42*, 8131–8139, doi:10.1002/2015GL065327.
- Liu, J., J. A. Curry, H. Wang, M. Song, and R. M. Horton (2012), Impact of declining Arctic sea ice on winter snowfall, *Proc. Natl. Acad. Sci. U.S.A.*, *109*, 4074–4079.
- Miyakoda, K., G. D. Hembree, R. F. Strikler, and I. Shulman (1972), Cumulative results of extended forecast experiments. I: Model performance for winter cases, *Mon. Weather Rev.*, *100*, 836–855.
- Mori, M., M. Watanabe, H. Shiogama, J. Inoue, and M. Kimoto (2014), Robust Arctic sea-ice influence on the frequent Eurasian cold winters in past decades, *Nat. Geosci.*, *7*, 869–873.
- Plumb, R. A. (1985), On the three-dimensional propagation of stationary waves, *J. Atmos. Sci.*, *42*, 217–229.
- Robinson, D. A., K. F. Dewey, and R. R. Heim (1993), Global snow cover monitoring: An update, *Bull. Am. Meteorol. Soc.*, *74*, 1689–1696.
- Scaife, A. A., et al. (2014), Skillful long-range prediction of European and North American winters, *Geophys. Res. Lett.*, *41*, 2514–2519, doi:10.1002/2014GL059637.
- Screen, J. A., and I. Simmonds (2010), The central role of diminishing sea ice in recent Arctic temperature amplification, *Nature*, *464*, 1334–1337.
- Simpson, I. R., M. Blackburn, and J. D. Haigh (2009), The role of eddies in driving the tropospheric response to stratospheric heating perturbations, *J. Atmos. Sci.*, *66*, 1347–1365.
- Song, Y., and W. A. Robinson (2004), Dynamical mechanisms for stratospheric influences on the troposphere, *J. Atmos. Sci.*, *61*, 1711–1725.
- Stroeve, J. C., M. C. Serreze, M. M. Hollan, J. E. Kay, J. Maslanik, and A. P. Barrett (2012), The Arctic's rapidly shrinking sea ice cover: A research synthesis, *Clim. Change*, *110*, 1005–1027.
- Tang, Q., X. Zhang, Z. Yang, and J. Francis (2013), Cold winter extremes in northern continents linked to Arctic sea ice loss, *Environ. Res. Lett.*, *8*, 014036, doi:10.1088/1748-9326/8/1/014036.
- Thompson, D. W. J., and J. M. Wallace (2000), Annular modes in the extratropical circulation. Part I: Month-to-month variability, *J. Clim.*, *13*, 1000–1016.
- Thompson, D. W. J., and J. M. Wallace (2001), Regional climate impacts of the Northern Hemisphere annular mode, *Science*, *293*, 85–89.
- Wilks, D. S. (2006), *Statistical Methods in the Atmospheric Sciences*, 2nd ed., Elsevier, Boston, Mass.

Supporting Information for  
**The Combined Influences of Autumnal Snow and Sea Ice on Northern Hemisphere Winters**

Jason C. Furtado  
School of Meteorology, University of Oklahoma, Norman, OK, USA

Judah L. Cohen  
Atmospheric and Environmental Research, Lexington, MA, USA

Eli Tziperman  
Dept of Earth and Planetary Sciences and School of Engineering and Applied Sciences, Harvard  
University, Cambridge, MA, USA

Introduction

The supplemental material includes two (2) Supplementary Figures for the manuscript (fs01.tiff and fs02.tiff) and one (1) Supplementary Table (SupplementalTable1.pdf). Below are the captions for those figures and table.

1. fs01.tiff

**Figure S1.** (a)-(c) As in Fig. 1 but the snow cover extent is restricted to Eurasia only. (d) (black) The leading principal component (PC) time series (standardized and inverted) from the multivariate EOF analysis in (a)-(c) from 1979/80-2014/15. (red) The observed DJF NAM 1000 hPa index from 1979/80 – 2014/15. Correlation between the two plotted indices is  $r = 0.80$  ( $p < 0.01$ ).

2. fs02.tiff

**Figure S2.** Composite of December - February (DJF) average near-surface temperature anomalies ( $^{\circ}\text{C}$ ) during years with high October SCE and low November SIE. (b) As in (a) but averaged for December. (c) As in (a) but averaged for January. (d) As in (a) but averaged for February. Years used for the composites shown in Table S1.

3. SupplementalTable1.pdf

**Table S1.** List of high and low snow cover and sea ice extent years used in the composite analyses in the study.

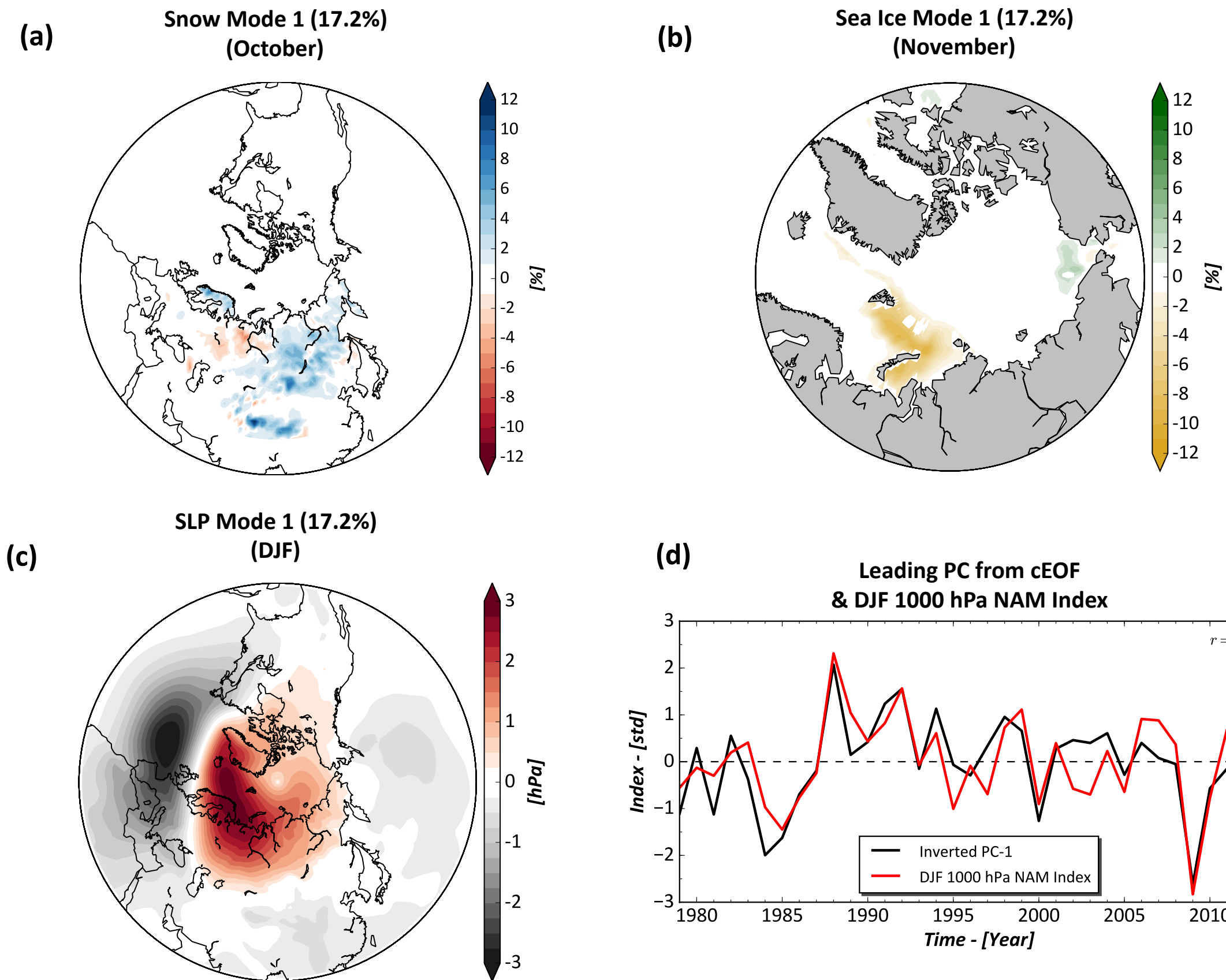


**Figure S1.** (a)-(c) As in Fig. 1 but the snow cover extent is restricted to Eurasia only. (d) (black) The leading principal component (PC) time series (standardized and inverted) from the multivariate EOF analysis in (a)-(c) from 1979/80-2014/15. (red) The observed DJF NAM 1000 hPa index from 1979/80 – 2014/15. Correlation between the two plotted indices is  $r = 0.80$  ( $p < 0.01$ ).

**Near-Surface Temperature Anomalies Composite**  
**for Years with High October SCE and Low November SIE**

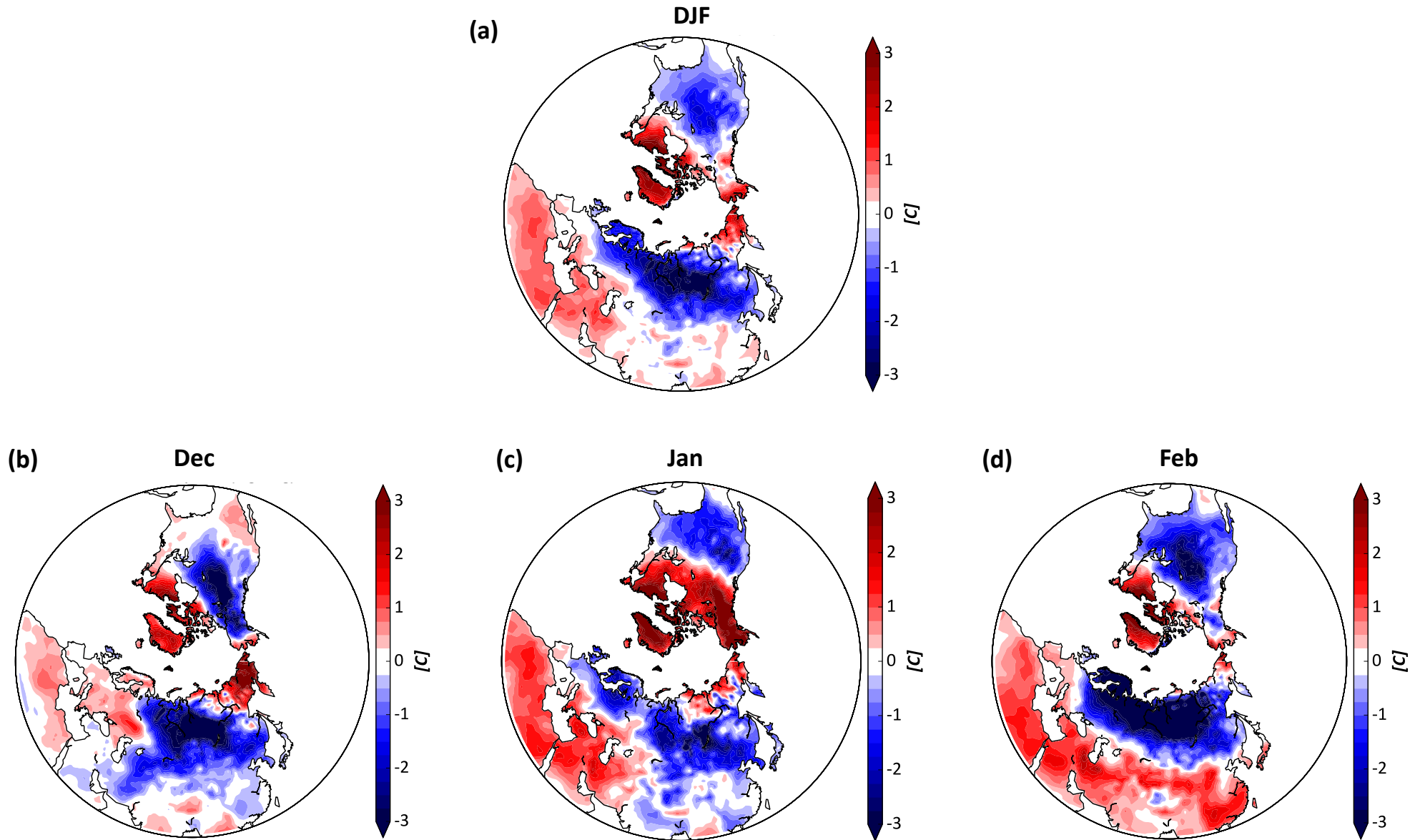


**Figure S2.** Composite of December - February (DJF) average near-surface temperature anomalies ( $^{\circ}\text{C}$ ) during years with high October SCE and low November SIE. (b) As in (a) but averaged for December. (c) As in (a) but averaged for January. (d) As in (a) but averaged for February. Years used for the composites shown in Table S1.

**Table S1.** List of high and low snow cover and sea ice extent years used in the composite analyses in the study.

High October Snow Cover Years	1984, 1999, 2000, 2002, 2006, 2009, 2010, 2012, 2013, 2014
Low October Snow Cover Years	1980, 1982, 1987, 1988, 1989, 1990, 1991, 1992, 1994, 1995
High November Sea Ice Extent Years	1980, 1982, 1988, 1990, 1991, 1992, 1994, 1997, 1998, 2002
Low November Sea Ice Extent Years	1984, 2000, 2006, 2007, 2008, 2009, 2010, 2011, 2012, 2013
High October Snow Cover <i>and</i> Low November Sea Ice Extent Years	1984, 2000, 2006, 2009, 2010, 2012, 2013
Low October Snow Cover <i>and</i> High November Sea Ice Extent Years	1980, 1982, 1988, 1990, 1991, 1992, 1994